A novel mouse model for familial hypocalciuric hypercalcemia (FHH1) reveals PTH-dependent and independent CaSR defects

Catharina J. Küng[1] · Arezoo Daryadel[1] · Rocio Fuente[1,2] · Betül Haykir[1] · Martin Hrabĕ de Angelis[3,4,5] · Nati Hernando[1] · Isabel Rubio-Aliaga[1] · Carsten A. Wagner[1]

Abstract

The Calcium-sensing receptor (CaSR) senses extracellular calcium, regulates parathyroid hormone (PTH) secretion, and has additional functions in various organs related to systemic and local calcium and mineral homeostasis. Familial hypocalciuric hypercalcemia type I (FHH1) is caused by heterozygous loss-of-function mutations in the *CaSR* gene, and is characterized by the combination of hypercalcemia, hypocalciuria, normal to elevated PTH, and facultatively hypermagnesemia and mild bone mineralization defects. To date, only heterozygous *Casr* null mice have been available as model for FHH1. Here we present a novel mouse FHH1 model identified in a large ENU-screen that carries an c.2579 T > A (p.Ile859Asn) variant in the *Casr* gene (*Casr*^BCH002 mice). In order to dissect direct effects of the genetic variant from PTH-dependent effects, we crossed *Casr*^BCH002 mice with PTH deficient mice. Heterozygous *Casr*^BCH002 mice were fertile, had normal growth and body weight, were hypercalcemic and hypermagnesemic with inappropriately normal PTH levels and urinary calcium excretion replicating some features of FHH1. Hypercalcemia and hypermagnesemia were independent from PTH and correlated with higher expression of claudin 16 and 19 in kidneys. Likewise, reduced expression of the renal TRPM6 channel in *Casr*^BCH002 mice was not dependent on PTH. In bone, mutations in *Casr* rescued the bone phenotype observed in *Pth* null mice by increasing osteoclast numbers and improving the columnar pattern of chondrocytes in the growth zone. In summary, *Casr*^BCH002 mice represent a new model to study FHH1 and our results indicate that only a part of the phenotype is driven by PTH.

Keywords Calcium-sensing receptor · Kidney · Bone · Parathyroid hormone · Fibroblast growth factor 23 · Mouse model

Catharina J. Küng, and Arezoo Daryadel share first authorship.

Isabel Rubio-Aliaga, and Carsten A. Wagner share last authorship.

✉ Carsten A. Wagner
  Wagnerca@access.uzh.ch

1 Institute of Physiology, University of Zürich, Winterthurerstrasse 190, CH-8057 Zurich, Switzerland

2 Department of Morphology and Cellular Biology, University of Oviedo, Oviedo, Spain

3 Institute of Experimental Genetics, Helmholtz Zentrum München, German Research Center for Environmental Health, Neuherberg, Germany

4 Lehrstuhl Für Experimentelle Genetik, Technische Universität München, Freising-Weihenstephan, Germany

5 Member of German Center for Diabetes Research (DZD), Neuherberg, Germany

Introduction

The Calcium-sensing receptor (CaSR) is a G protein-coupled receptor that senses extracellular concentrations of ionized calcium [14]. The CaSR forms homodimers and is highly expressed in several tissues central to the regulation of systemic calcium homeostasis including parathyroid glands, bone, cartilage, various segments of the gastrointestinal tract, and kidneys. In parathyroid glands, the CaSR regulates the synthesis and secretion of parathyroid hormone (PTH) suppressing PTH release when ionized calcium concentrations are high. In kidney, CaSR is expressed at the basolateral membrane of cells of the thick ascending limb of the loop of Henle (TAL) where it regulates paracellular calcium and magnesium reabsorption mediated by claudin 16 (cdn16) and claudin 19 (cldn19). Under conditions of elevated calcium, the CaSR downregulates clnd16 and 19 in part through

enhancing claudin 14 (cldn14) which inhibits cldn16 and cldn19 [14]. These effects of the CaSR are PTH-independent [18, 22]. Stimulation of CaSR activity may also inhibit the $Na^+/K^+/2Cl^-$ -cotransporter NKCC2 in TAL cells. Also, NCC activity may be regulated by the CaSR [6]. Whether the CaSR is also localized to other nephron segments has remained controversial [13, 22, 25]. In proximal tubule, CaSR may inhibit bicarbonate reabsorption via the NHE3 Na^+/H^+-exchanger and phosphate reabsorption by the NaPi-IIa cotransporter [2, 5]. Also, inhibition of AQP2-mediated water reabsorption and stimulation of H^+-ATPase activity in the collecting duct system has been suggested [24, 27].

Familial hypocalciuric hypercalcemia type I (FHH1, OMIM: #145980) is a genetic disorder characterized by hypercalcemia, hypocalciuria, normal to mildly elevated PTH levels, and in some patients mildly reduced bone mineral density and hypermagnesemia [14]. FHH1 is caused by heterozygous loss-of-function mutations in the gene encoding the CaSR [14, 21]. Heterozygous Casr KO mice have been described as a model of FFH1 but only partially characterized [15].

The $Casr^{BCH002}$ mouse line has been identified in a large N-ethyl-N-nitrosourea (ENU)-driven mutagenesis screen searching for bone-related parameters that included alkaline phosphatase, total calcium, and inorganic phosphate [26]. Heterozygous $Casr^{BCH002}$ mice had normal alkaline phosphatase but elevated plasma total calcium and lower phosphate. Histological analysis of the line revealed enlarged parathyroid glands and higher median PTH levels. Genetic analysis identified a c.2579 T > A (p.Ile859Asn) variant in the CaSR. This variant, affecting a residue within a transmembrane region of the CaSR [16], is listed in the ClinVar database as a variant of uncertain significance while the SIFT structure tool (https://sift.bii.a-star.edu.sg/) lists it as deleterious. Thus, the structural predictions together with the already known phenotype suggest that $Casr^{BCH002}$ mice may be a model for FHH1.

The aims of this study were to examine whether $Casr^{BCH002}$ mice are a model of FHH1 and whether some of the phenotypic changes of $Casr^{BCH002}$ mice were dependent on PTH. To this end, we examined not only $Casr^{BCH002}$ mice but also Pth KO and $Casr^{BCH002}/Pth$ KO mice.

Materials and methods

Animals

The generation, breeding, and genotyping of PTH deficient mice has been described previously [9, 19]. Pth null mice were in a pure C57BL/6 J background. BCH002 mice, harboring a putatively inactivating mutation in the $Casr$ gene, were derived from an ENU-based genetic screen

[26]. Genetic analysis of the line identified a heterozygous c.2579 T > A, p. Ile859Asn mutation in the $Casr$ gene ($Casr^{BCH002}$). $Casr^{BCH002}$ mice were originally in C3HeB/FeJ background and crossed with Pth heterozygous over three generations to yield all desired genotypes with a mixed background. To evaluate the effect of the CaSR on renal function independent from PTH, heterozygous BCH002 and Pth null mice were crossed and further bred resulting in 4 different genotypes: wildtype for both genes (WT/WT), heterozygous for the $Casr^{BCH002}$ mutation (WT/ $Casr^{BCH002}$), homozygous for PTH deficiency (Pth KO) (Pth KO/WT), and heterozygous for the $Casr^{BCH002}$ mutation and homozygous for Pth deficiency (Pth KO/ $Casr^{BCH002}$). All mice used were littermates and had a mixed C3H-C57 background. Only male mice were used at the age of 8–10 weeks.

All experiments were performed according to Swiss Animal Welfare laws and approved by the local veterinary authority (Kantonales Veterinäramt Zürich) under the numbers ZH156/16 and ZH240/19.

Determination of urinary and plasma metabolites Urinary and plasma levels of total calcium, inorganic phosphate (Pi) and creatinine (enzymatically for plasma) were measured on a UniCel DxC 800 Synchron Clinical System (Beckman Coulter) in the Zurich Integrative Rodent Physiology (ZIRP) facility. Blood levels of ionized calcium were measured with a blood-gas analyzer (Epoc blood gas analysis system, Siemens, Germany). Plasma levels of intact FGF23 (Immutopics; #60–6800), the C-terminal FGF23 fragment (Immutopics; #60–6300) and PTH (Immutopics; #60–2305) were determined by ELISA according to the manufacturer's protocols.

Protein extractions and preparation of brush border membranes (BBM) For the extraction of total proteins, kidneys were homogenized in RIPA buffer containing 50 mM Tris–HCl (pH 7.4), 150 mM NaCl, 1% NP-40 and 0.5% Deoxycholate acid sodium salt, supplemented with Phenylmethylsulfonyl fluoride (PMSF) and protease inhibitor cocktail (Complete; Roche Diagnostics, Basel, Switzerland). The homogenate was centrifuged at 2000 rpm for 20 min at 4 °C. The resulting supernatant was further centrifuged at 41,000 rpm for 1 h at 4 °C in order to enrich the membrane proteins in the final pellet. Renal BBM were prepared according to the Mg^{2+} precipitation technique [3]. BBM were resuspended in 300 mM Mannitol, 20 mM HEPES-Tris, pH 7.4 and stored at -20 °C. Protein concentrations were determined with the Bio-Rad Protein Assay (Bio-Rad, Hercules, CA).

Immunoblotting The expression levels of transporter proteins were quantified on either total membrane extractions or BBM, while calbindin D28k and Cyp24a1 were determined in total protein extractions. To this end, 10 μg of BBM or 50 μg of either total membrane or total protein were

solubilised in Laemmli buffer and separated on SDS-PAGE and transferred to polyvinylidene difluoride membranes (EMD Millipore, Billerica, MA). After blocking nonspecific binding with 5% milk powder in Tris-buffered saline containing 0.1% Tween-20 for 1 h, the blots were incubated overnight at 4 °C with the primary antibodies. Antibodies used were directed against NaPi-IIa (1:2000) [8], NaPi-IIc (1:1000) [20], total NCC (1:2000; a kind gift of J. Loffing [17]), NKCC2 (1:2000, a kind gift of J. Loffing) [31], NHE3 (1:1000; StressMarq; SPC-400D), TRPV5 (1: 500, a kind gift by O. Bonny, [29]), TRPM6 (1:2000, a kind gift by J. Loffing, [28]), the vitamin D receptor (Vdr) (1:500 Santa Cruz), Cyp24a1 (1:1000, Proteintech), the Ca^{2+}-sensing receptor (CaSR) (1:500, Thermo Fisher) and calbindin D28k (1:500, Swant). After washing and further blocking, blots were incubated with the appropriate secondary antibodies for 1 h at room temperature. Finally, membranes were exposed to chemiluminescent substrate for 5 min, and protein signals were detected on a LAS-4000 Luminescent Image Analyzer. All images were quantified with Advanced Image Data Analyzer (AIDA; Raytest). The expression of the proteins of interest was normalized to the Ponceau signal.

Micro-computer tomography Right tibias stored at -80 °C were defrosted and scanned with a µCT40 (Scanco Medical, Wangen-Brüttisellen, Switzerland), following the manufacturer's instructions. Briefly, whole tibia and distal epiphysis were imaged using 20 mm or 5 mm fields of view, respectively, at a tube current of 100 µA, 90 kV tube voltage and 3 min scan time. A 3D Gaussian filter (sigma 0.8, support 1) was applied to reduce the noise present in the images. A 1200 mg/cm^3 hydroxy-apatite phantom from the company was used to translate greyscales into bone mineral density (BMD). BMD and bone volume data were assessed with the Analyze 12.0 program (Analyze Direct, Inc). We analyzed the bone parameters following previously published guidelines [4].

Histomorphometry After µCT analysis, the right tibia was fixed in 4% paraformaldehyde (PFA), decalcified in 10% EDTA for 3 to 4 weeks and embedded in paraffine. Five µm sections were deparaffinized and washed with PBS for histological analysis. For tartrate-resistant acid phosphatase (TRAP) staining, two slides per animal were incubated in Tris–HCl 0.2 M pH 9.5 for 45 min at 37 °C, and then for 15 min following the TRAP kit instructions (Sigma 387A-1KT). We evaluated the number and/or area of active osteoclasts per total area. Alcian blue safranin (AAS) staining and alkaline phosphatase (ALP) staining were performed as previously described [11, 30]. With the AAS staining we evaluated the growth plate height and the height of the different zones. On the ALP-stained sections the intensity of the staining in triplicates was evaluated by an examiner blinded to the genotype and a score of the staining intensity

was given: negative (0), weak (1), moderate (2), and strong (3). Pictures were made using a digital microscope camera (Olympus E-330 and Olympus BX41; Olympus). Evaluation of the images was performed using the special bone-imaging program Osteo (v. 2013; Bioquant Image Analysis Corporation, Nashville TN, USA).

Semi-quantitative real-time PCR Total RNA was isolated from kidney using a RNeasy kit (Qiagen, Basel, Switzerland). Bone RNA was isolated form one frozen tibia. Prior to freezing, the epiphysis was cut, and bone marrow was flushed out by centrifugation. Frozen bones were crushed in liquid nitrogen using a mortar. Then, RNA was extracted with Trizol (Invitrogen), followed by phenol–chloroform phase separation. RNA purification was done in all cases using the NucleoSpin RNA kit (Macherey–Nagel). RNA was reverse transcribed with TaqMan Reverse Transcription Kit (Applied Biosystems) after which cDNA was amplified by qPCR using Kapa mix (Sigma-Aldrich) with reporter tagged probes together with forward and reverse primers (Supplementary Table 1). Mouse primers and probe were designed using Primer Express (Applied Biosystems, USA) and purchased from Microsynth, Switzerland. Probes were labelled with the reporter dye FAM at the 5′ end and the quencher dye TAMRA at the 3′ end. The specificity of the primer was tested using adult mouse kidney or tibia cDNA by conventional PCR. Each pair of primer resulted only in a single band of the expected size (data not shown). qPCR reactions were performed on a 7500 Fast Real Time PCR System. Gene expression was normalized to HPRT or GAPDH and the obtained data was analyzed with the 7500 Fast Real-Time PCR System Sequence Detection Software v1.4. The relative gene expression was calculated according to the formula $2^{(Ct\,(control)\,-Ct\,(gene\,of\,interest))}$.

Statistics Statistical analyses were performed using Graph-Pad Prism version 9.3.1 for Windows (GraphPad Software, San Diego, California USA, http://www.graphpad.com). Statistical significance, defined as $P < 0.05$, was calculated using two-way ANOVA followed by multiple comparisons using the Tukey method. P values are displayed as: * $P < 0.05$, ** $P < 0.01$, *** $P < 0.001$, **** $P < 0.0001$. Data are presented as mean ± SEM.

Results

Aberrant mineral balance in Casr^BCH002 mice is independent from PTH

We characterized the mineral metabolism of BCH002 mice carrying the c.2579 T > A, p. Ile859Asn mutation in the *Casr* gene and its dependence on PTH. For that, we

analyzed four groups of male littermates: mice wildtype for both genes (WT/WT), mice deficient for PTH (*Pth* KO/WT), mice carrying one mutated allele in the *Casr* gene (WT/ *Casr* BCH002), and mice deficient for PTH and with one mutant *Casr* allele (*Pth* KO/ *Casr* BCH002). Mice carrying the homozygous *Casr*BCH002 mutation were not viable (data not shown). No or little differences were observed between the 4 groups regarding body weight, tibia and nose-tail length, food and water intake and urine and feces excretion (Supplementary Fig. 1). Plasma total calcium was elevated in *Casr* mutant mice regardless of the presence or absence of PTH (Fig. 1A). Ionized calcium was higher in *Pth* KO/*Casr* BCH002mice than in *Pth* KO/WT animals (Fig. 1B). Plasma Pi levels showed a trend to lower values in *Pth* KO/*Casr* BCH002 than in *Pth* KO/WT mice (Fig. 1C), while plasma magnesium was slightly elevated in these animals (Fig. 1D). Despite hypercalcemia in *Casr* mutant mice, urinary excretion of calcium was similar between groups, i.e. inappropriately normal in hypercalcemic *Casr* mutant mice (Fig. 1E). Urinary Pi excretion was higher in *Pth* KO/WT and WT/*Casr* BCH002 animals when compared to WT/WT mice, and persisted in *Pth* KO/*Casr* BCH002 mice (Fig. 1F). Urinary magnesium excretion was elevated in WT/*Casr*BCH002 mice when compared to WT/WT and *Pth* KO/*Casr* BCH002 mice (Fig. 1G). WT/*Casr*BCH002 mice had inappropriately comparable PTH levels to WT/WT while only very low PTH signals were detected in mice lacking PTH possibly due to some cross-reactivity of the PTH ELISA kit used (Fig. 1H). Intact and the C-terminal fragment of FGF23 were both elevated due to *Casr* mutations (Fig. 1I, J), also in the absence of PTH. Thus, mutant *Casr* mice show features of familial hypocalciuric hypercalcemia with evidence for primary hyperparathyroidism.

Altered renal expression of CaSR targets in Casr^BCH002 mice

Next, we examined the renal expression of transcripts and proteins regulated by CaSR or involved in renal calcium and Pi handling. Claudin 14 mRNA was similarly low expressed in all four genotypes (Fig. 2A), while claudin 19 and 16 mRNA were higher in WT/*Casr*BCH002 animals when compared to WT/WT, with a similar trend in *Pth* KO/*Casr*BCH002 mice (Fig. 2B, J). mRNA abundance of Egr1, a target gene of FGF23, was higher in *Casr* mutant mice (Fig. 2D) consistent with elevated FGF23 levels (Fig. 1I, J) in these mice. mRNA expression of Cyp27b1, the enzyme catalyzing the hydroxylation of calcidiol to calcitriol, was similarly low in all groups of mice

(Fig. 2E), but Cyp24a1 and the vitamin D receptor (Vdr) transcripts showed higher values in WT/*Casr*BCH002 mice compared to WT/WT (Fig. 2F, G). However, protein abundance of Cyp24a1 was elevated only in *Pth* KO/*Casr*BCH002 mice as compared to *Pth* KO/WT (Fig. 2H, I), while Vdr protein expression was similar in all groups (Fig. 2J, K).

Renal protein abundance of CaSR was clearly elevated in mutant mice, though it reached statistical significance only in the presence of PTH (Fig. 3A, B). The cleaved product of the Pi cotransporter NaPi-IIa and the NaPi-IIc cotransporter showed a small reduction in *Pth* KO/*Casr*BCH002 mice compared to WT/*Casr*BCH002 mice (Fig. 3C–G). The Na$^+$/H$^+$ exchanger NHE3 was reduced in *Casr* mutant mice and in mice lacking PTH, when compared to WT/WT mice (Fig. 3H, I).

Next, we assessed the abundance of several proteins involved in renal salt and calcium handling in the thick ascending limb of the loop of Henle, the distal convoluted tubule and connecting tubule. We found no alterations in the expression of the Na/K/2Cl-cotransporter NKCC2, the thiazide-sensitive NaCl-cotransporter NCC, the calcium channel TRPV5, and the calcium-buffering protein calbindin D28k (Fig. 4A–H). In contrast, the magnesium channel TRPM6 was reduced in *Casr* mutant mice in the absence of PTH (Fig. 4I, J).

Bone phenotype

In a last series we assessed bone in the four groups of mice. We first analyzed the mRNA abundance of various bone markers and factors involved in FGF23 synthesis. Higher circulating levels of intact FGF23 in *Casr* mutant mice did not correlate with increased *Fgf23* gene expression, but correlated with higher mRNA abundance of *Galnt3*, the enzyme stabilizing FGF23 through O-Glycosylation, in the WT/*Casr*BCH002 group (Fig. 5A, B). Small differences in mRNA abundance were found for *Nurr1*, a transcription factor involved in FGF23 regulation, and *Dmp1*, a negative regulator of FGF23. Both were elevated in *Pth* KO/*Casr*BCH002 mice compared to *Pth* KO/WT suggesting an effect of mutant Casr (Fig. 5C, D). Phex, another negative regulator of FGF23 showed no differences between the groups (Fig. 5E). We also found an increase in *Alp*, alkaline phosphatase, a marker of osteoblasts (Fig. 5F), in WT/*Casr*BCH002 mice and a decrease in *Rnx2*, a marker of osteoclasts, in WT/*Casr*BCH002 (nonsignificant) and *Pth* KO/*Casr*BCH002 (significant) mice suggesting a change in the balance between osteoblasts and osteoclasts (Fig. 5G). No differences were found between the groups in *Opg* and *Rankl* mRNA abundance, markers of bone formation and resorption (Fig. 5H, I).
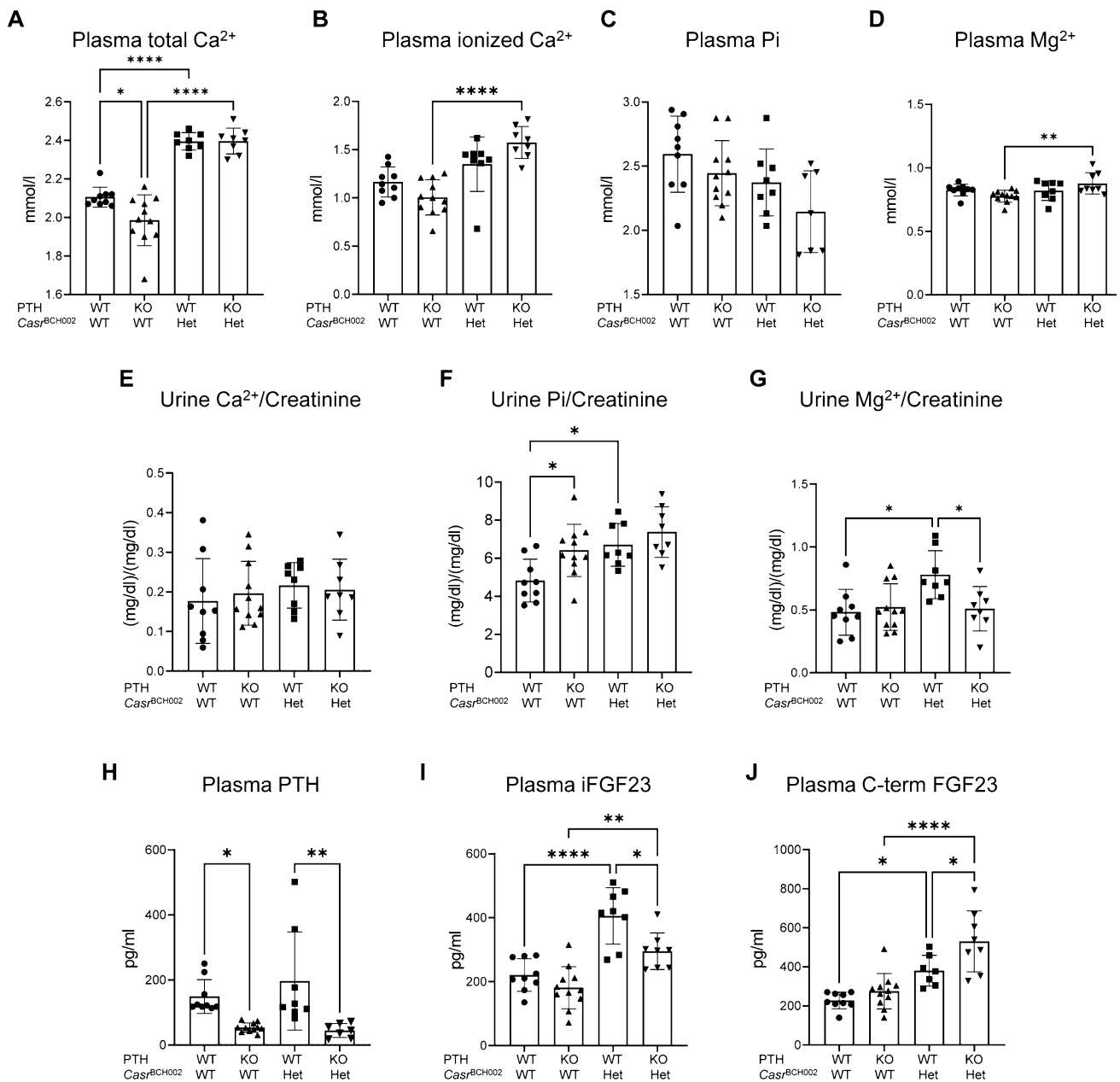
Fig. 1 Parameters of mineral metabolism. Plasma and urine analysis for parameters of phosphate and calcium homeostasis in wildtype (WT/WT), *Pth* KO/*Casr*[BCH002], WT/ *Casr*[BCH002] and *Pth* KO/*Casr*[BCH002] mice. Measurements in plasma of (**A**) total calcium, (**B**) ionized Ca^{2+}, (**C**) phosphate (Pi), (**D**) magnesium (Mg^{2+}). Urinary excretion of (**E**) Ca^{2+}, (**F**) phosphate (Pi), and (**G**) Mg^{2+}, all normalized to creatinine. Plasma values of (**H**) PTH, (I) intact FGF23 (iFGF23), and (**J**) C-terminal FGF23 (C-term FGF23). All data were analysed in groups of $n = 7$–11 animals. Values are presented with means ± SD together with single values. Data were analysed with 2-way ANOVA with Tukey correction for multiple comparisons between PTH and BCH genotypes. * $p < 0.05$, ** $p < 0.01$, **** $p < 0.0001$

Also no differences were observed in the mRNA abundance of CaSR (Fig. 5J).

Histomorphology was used to analyze the growth plate of tibias (Fig. 6A). Absence of PTH caused a profound

disturbance of the columnar pattern of chondrocytes in the growth zone which was less visible in *Casr* mutant animals (WT/*Casr*[BCH002]), and this disturbance was even partially restored by the *Casr* mutation in *Pth* KO/*Casr*[BCH002] mice
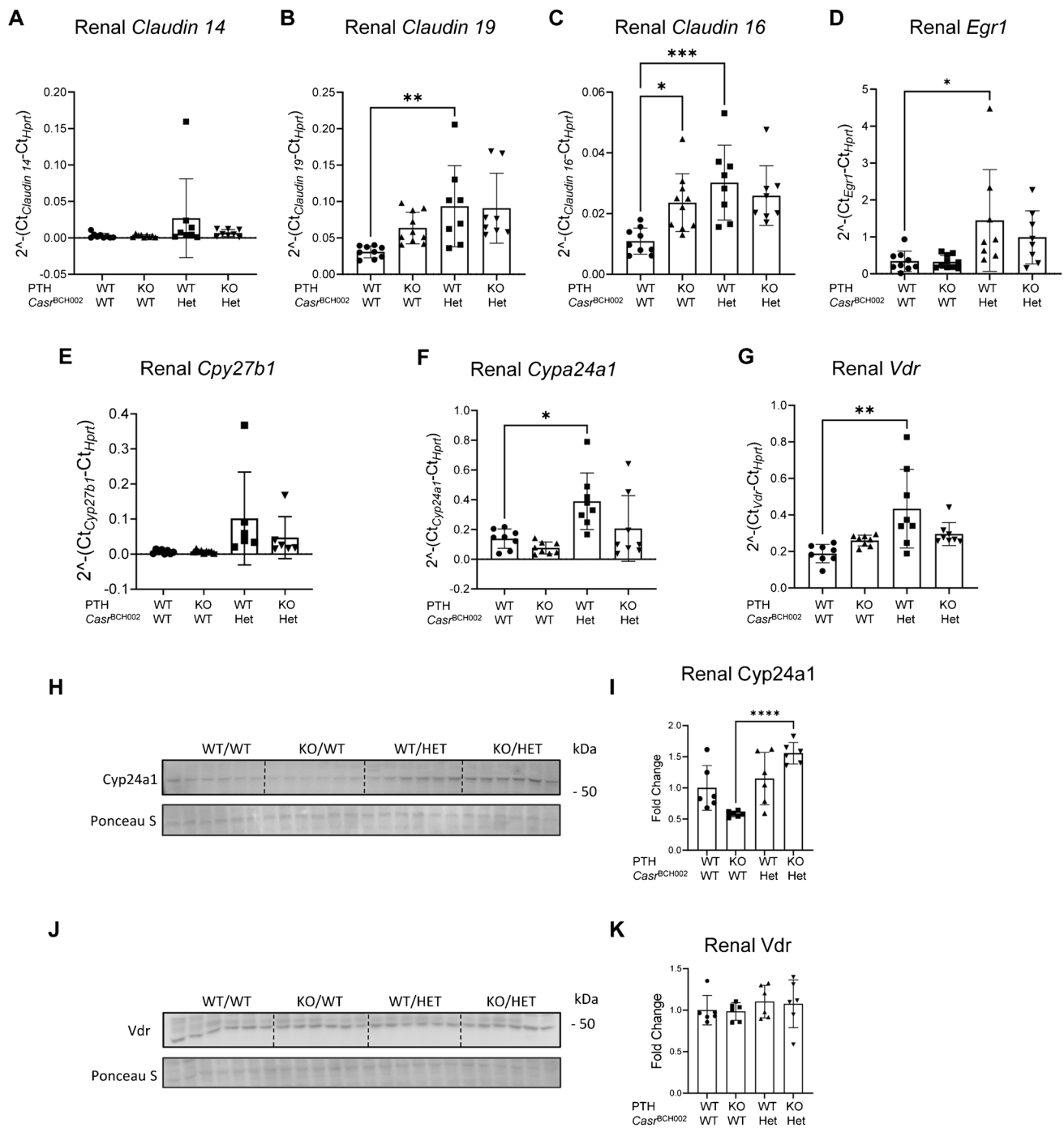
Fig. 2 Renal abundance of claudins, Egr1, and calcitriol metabolizing enzymes and vitamin D receptor. mRNA expression and protein abundance was analysed by real time qPCR or immunoblotting in kidneys from wildtype (WT/WT), *Pth* KO/*Casr*[BCH002] WT, WT/*Casr*[BCH002] and *Pth* KO/*Casr*[BCH002] mice. mRNA expression of (**A**) *claudin14*, (**B**) *claudin19*, (**C**) *claudin16*, (**D**) *egr1*, (**E**) *1-α-hydroxylase* (*Cyp27b1*), (**F**) *24-hydroxylase* (*Cyp24a1*), and (**G**) *vitamin D receptor* (*Vdr*) were assessed relative to the housekeeping gene *Hprt*. Protein expression of (**H**, **I**) Cyp24a1 (60 kDa) and (**J**, **K**) Vdr (47 kDa) were normalized to Ponceau S staining. Values are presented as means $\pm$ SD ($n = 8$–10) together with single values. Data were analysed with 2-way ANOVA with Tukey correction for multiple comparisons between PTH and BCH genotypes. * $p < 0.05$, ** $p < 0.01$, *** $p < 0.001$, **** $p < 0.0001$
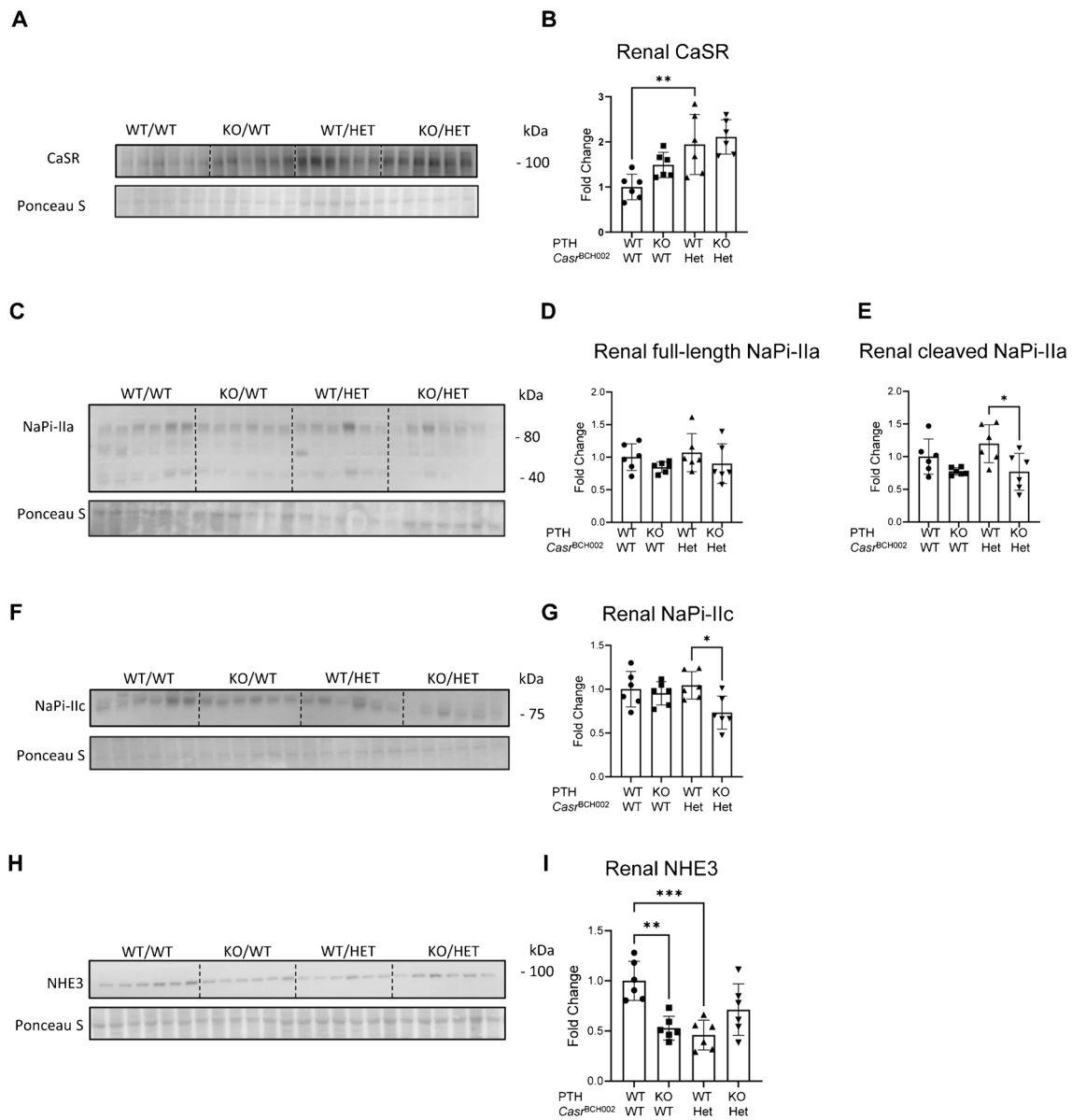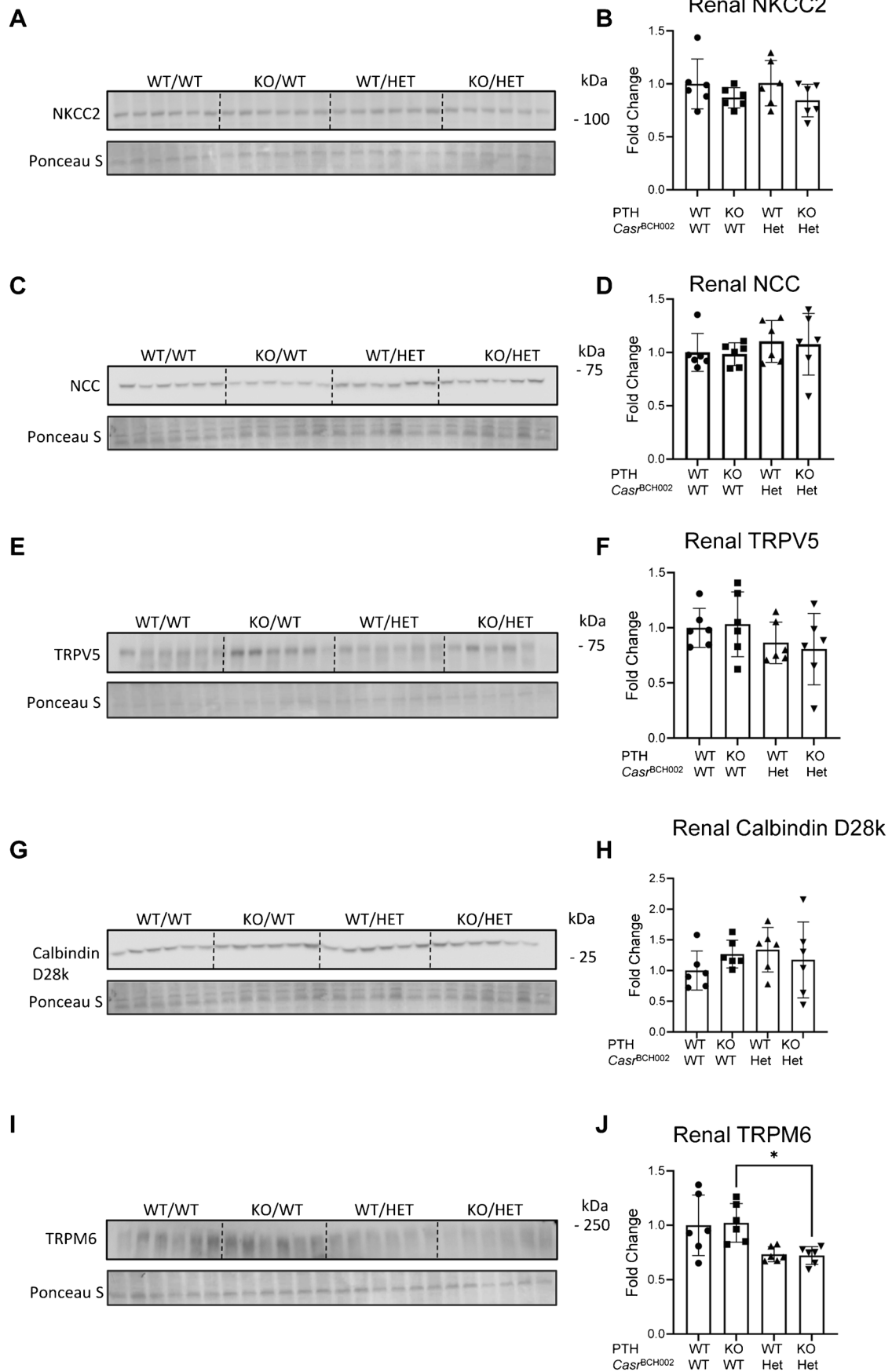
Fig. 3 Expression of key proteins involved in renal calcium and phosphate handling. Protein abundance was assessed by immunoblotting in total homogenates (Casr) or brush border membranes (NaPi-IIa, NaPi-IIc and NHE3) from kidneys of wildtype (WT/WT), *Pth* KO/*Casr*[BCH002], WT/*Casr*[BCH002] and *Pth* KO/*Casr*[BCH002] mice. Protein expression of (**A**, **B**) CaSR (130 kDa), (**C–E**) NaPi-IIa (full length 85 kDa and cleaved COOH-terminal fragment 45 kDa), (**F**, **G**) NaPi-IIc (80 kDa), and (**H**, **I**) Na$^+$/H$^+$-exchanger isoform 3 (NHE3, 93 kDa) were normalized to the corresponding ponceau S staining. Values are presented as means $\pm$ SD together with single values ($n = 6$). Data were analysed with 2-way ANOVA with Tukey correction for multiple comparisons between PTH and BCH genotypes. * $p < 0.05$, ** $p < 0.01$, *** $p < 0.001$

◀**Fig. 4** Expression of key proteins involved in renal calcium, magnesium, and salt handling. Protein abundance was assessed by immunoblotting in protein homogenates from kidneys from wildtype (WT/WT), *Pth* KO/*Casr*^BCH002^, WT/*Casr*^BCH002^ and *Pth* KO/*Casr*^BCH002^ mice. Protein expression of (**A**, **B**) NKCC2 (120 kDa), (**C**, **D**) NCC (130 kDa), (**E**, **F**) TRPV5 (75 kDa) (**G**, **H**) Calbindin D28k (28 kDa), and (**I**, **J**) TRPM6 (230 kDa) were normalized to the corresponding ponceau S staining. Values are presented as means ± SD together with single values (*n* = 6/group). Data were analysed with 2-way ANOVA with Tukey correction for multiple comparisons between PTH and BCH genotypes. * $p < 0.05$

(Fig. 6A). Similarly, the increase in the ratio of hypertrophic to growth plate height zone associated with PTH depletion was rescued in *Pth* KO/*Casr*^BCH002^ mice when

compared to *Pth* KO/WT mice (Fig. 6B). ALP positive was present only in the deep layers of articular cartilage adjacent to the subchondral bone. No differences were observed in the intensity and distribution of osteoblasts (Fig. 6C). The number of osteoclasts was highly increased in the absence of PTH and this increase was partly blunted by the *Casr* mutant animals (Fig. 6D). The *Casr* mutation had no effect on osteoclasts surface neither in the presence nor in the absence of PTH (Fig. 6E).

We further analyzed bone by μCT. Despite the changes in bone morphology, no major alterations were observed by μCT analysis in bone between the groups (Supplementary Table 2).
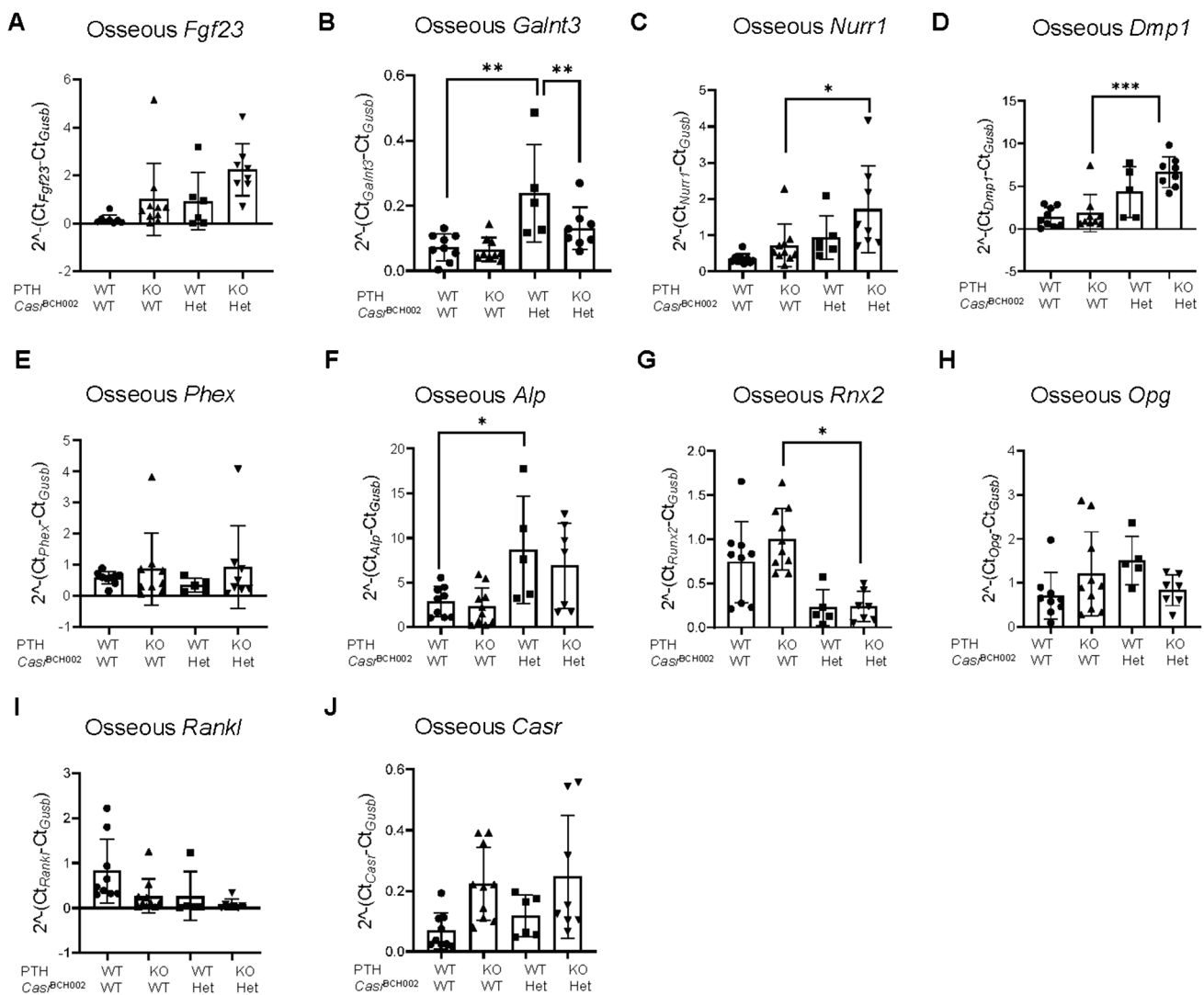

Fig. 5 mRNA expression of bone markers in tibia. mRNA expression was analysed by RT-qPCRs in tibias from wildtype (WT/WT), *Pth* KO/*Casr*^BCH002^, *Pth* WT/*Casr*^BCH002^ and *Pth* KO/*Casr*^BCH002^ mice. (**A**) *Fgf23*, (**B**) *Galnt3*, (**C**) *Nurr-1*, (**D**) *Dmp1*, (**E**) *Phex*, (**F**) *Alp*, (**G**) *Rnx2*, (**H**) *Opg*, (**I**) *Rankl*, (**J**) *Casr* relative to the housekeeping gene *Gusb*. Values are presented as means ± SD together with single values (*n* = 8–10). Data were analysed with 2-way ANOVA with Tukey correction for multiple comparisons between PTH and BCH genotypes. * $p < 0.05$, ** $p < 0.01$, *** $p < 0.001$
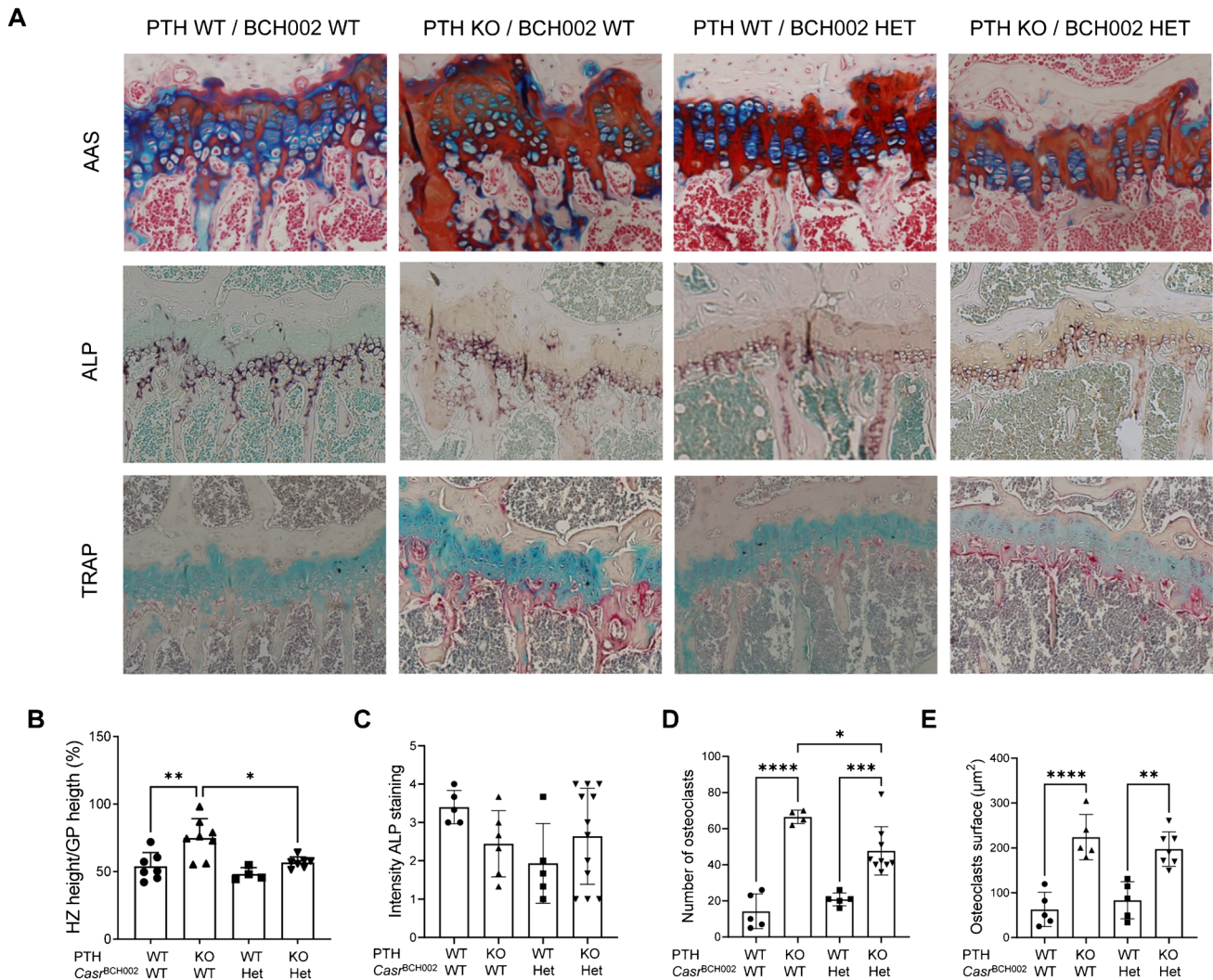
Fig. 6 Analysis of tibia growth plate. The growth plate of tibias from wildtype (WT/WT), *Pth* KO/*Casr*[BCH002], WT/*Casr*[BCH002] and *Pth* KO/*Casr*[BCH002] mice was analyzed using immunohistochemistry. (**A**) Upper panels: Alcian blue safranin (AAS) staining for mature cartilage (red) and connective tissue (blue):; middle panels: alkaline phosphatase (ALP, purple) to identify osteoblasts and counterstain of tissue (green), and lower panels: Tartrate-resistant alkaline phosphate (TRAP) to identify osteoclasts (pink). Blue staining for connective tissue and nuclei stained in purple. Morphometric analysis of (**B**) the ratio between the hypertrophic zone (HZ) and growth plate (GP), (**C**) the intensity of ALP staining, (**D**) number of osteoclasts, and (**E**) the surface covered by osteoclasts. Values are presented as means $\pm$ SD ($n=5$). Data were analysed with 2-way ANOVA with Tukey correction for multiple comparisons between PTH and BCH genotypes. * $p < 0.05$, ** $p < 0.01$, *** $p < 0.001$, **** $p < 0.0001$

Discussion

In this study we present a new mouse model for familial hypocalciuric hypercalcemia (FHH1) due to an inactivating *Casr* mutation and analyze to which extent the phenotype is dependent on PTH. Major signs of FHH1 include hypercalcemia, hypocalciuria, normal to elevated PTH, and variably hypophosphatemia, hypermagnesemia, and mild bone mineralization defects. We thus focused our examinations on these aspects. FFH is a relatively benign disorder due to dominant loss-of-function variants in the *Casr* gene [14, 21]. The *Casr*[BCH002] mice were identified in a large ENU-mutagenesis screen based on hypercalcemia and hypophosphatemia [26]. However, the latter was only present in half of the animals. Mutant mice had been reported to have also slightly elevated PTH levels and enlarged parathyroid glands [26]. The mutation was mapped to the *Casr* locus and a c.2579 T > A, (p. Ile859Asn) variant detected. This mutation is located in the transmembrane region of the Casr protein and is predicted to impair function of the CaSR. Whether the mutation exerts a dominant negative effect or the phenotype of mice is due to haploinsufficiency of the *Casr* gene remains unclear at this point. The initial mouse line had already been crossed back for more than 15 generations likely diluting possible

other bystander variants caused by ENU [26]. We crossed the line further over at least three more generations into *Pth* KO mice. Of note, the initial line had been in the C3HeB/FeJ background while *Pth* KO mice were in a C57BL/6 J background. Thus, our mouse line is in a mixed background and we strictly used only littermates for experiments. The changes in genetic background and standard rodent chow used in our facility may also explain some minor differences in phenotype between the initial description of the BC002 line and our findings discussed below.

Casr^BCH002 mice recapitulate several features of FHH1 including hypercalcemia, an inappropriately normal PTH which is higher than expected for the degree of hypercalcemia. We also found inappropriately normal urinary calcium excretion which is lower than expected for hypercalcemia, and hypermagnesemia. It has been suggested that elevated FGF23 levels may distinguish FHH1 from other forms of PTH-dependent hypocalciuric hypercalcemia [1]. Our mouse model showed higher intact FGF23 levels and this was persistent in the absence of PTH. Likewise, the C-terminal fragment of FGF23 is higher in *Casr*^BCH002 mutant animals with and without PTH. In WT/*Casr*^BCH002 mice we also found higher *Galnt3* mRNA in bone which serves to stabilize FGF23. In mice lacking both the Casr and PTH manipulations of calcium and phosphate caused increases in FGF23 only when the calcium-phosphate product (Ca x Pi) exceeded a threshold [23]. The mechanism sensing the Ca x Pi remains elusive.

The CaSR regulates PTH secretion by the parathyroid glands. Reduced activity of the CaSR shifts the relationship between ionized calcium and PTH to the right (i.e., suppression of PTH release requires higher calcium levels) as also apparent in the Casr^BCH002 mice. Since PTH is a major hormone regulating calcium, phosphate, and bone metabolism, we asked whether some of the features of FHH1 might be dependent on PTH. Several findings suggest that part of the phenotype is independent from PTH, namely hypercalcemia, and higher FGF23 (both intact and C-terminal fragment). In kidney, the transcriptional upregulation of cldn16 and cldn19 as well as the downregulation of NHE3 and TRPM6 protein expression are independent from PTH. Moreover, upregulation of Galnt3 and downregulation of Rnx2 transcripts in bone are independent of PTH. In the sole absence of PTH, osteoclast numbers were increased while in *Casr*^BCH002 mutant mice without PTH, this increase was partly blunted. Thus, several of the key features of FHH1 are unrelated to PTH but appear to be caused by mutant *Casr*. Whether all these phenotypes are directly linked to mutant *Casr* or indirectly, e.g. via elevated FGF23 (e.g. phosphaturia) or hypermagnesemia (e.g. lower TRPM6 levels) remains to be established. Our data are also consistent with findings in rats demonstrating a PTH-independent regulation of renal calcium handling by the CaSR [18] which may contribute also to the phenotype observed in *Casr*^BCH002 mice.

Previously, homo- and heterozygous *Casr* KO mice have been generated. While the full ablation of the *Casr* mimics neonatal severe hyperparathyroidism, heterozygous mice have been suggested as model for FHH1 [15]. These heterozygous mice have higher total and ionized blood calcium with elevated PTH levels. Moreover, serum magnesium was higher. Urinary calcium excretion in spot urine appeared to be reduced. Our *Casr*^BCH002 mice recapitulate most of these findings except for PTH, however, Ho et al. had measured PTH after an overnight fasting while our mice were fed a libitum. Of note, the phenotype in our mice is less severe than in mice totally lacking Casr which might argue for either only a milder effect of the specific Ile859 Asn mutation with no dominant negative effect or for haploinsufficiency. The latter would be compatible with electrolyte disorders similar to the heterozygous mice. Heterologous expression studies of the mutant receptor may be needed to address this question. Unfortunately, no information is available as to the further phenotype of heterozygous Casr null mice, while our data demonstrate distinct effects in bone and kidney.

It has been debated whether the CaSR is expressed in the renal proximal tubule [5, 18, 25] and it has been suggested that the CaSR may stimulate bicarbonate absorption in the proximal tubule involving the Na$^+$/H$^+$-exchanger NHE3 [5]. In the *Casr*^BCH002 mice we found a downregulation of NHE3 which might be explained by the absence of normal CaSR signaling. However, also in *Pth* KO mice and in the *Pth* KO/ *Casr*^BCH002, NHE3 was downregulated. PTH has been shown to increase internalization and downregulation of NHE3 [7, 12] and that downregulation of NHE3 reduced proximal tubule calcium reabsorption [10]. Thus, the mechanism leading to downregulation of NHE3 in the absence of PTH remains to be established.

In bone, we found no major effect of the *Casr*^BCH002 mutation except on Alp and Rnx2 mRNA expression. The differences in Alp mRNA, however, did not translate into changes in ALP staining in bone sections. The decrease in Rnx2 in animals with mutant CaSR might suggest a problem in osteoblast formation or differentiation. However, no differences in ALP staining suggest similar osteoblast numbers. In contrast, TRAP stainings suggest that the absence of PTH is associated with higher osteoclast numbers which is surprising as PTH is a major stimulus for the formation of osteoclasts. MicroCT analysis of femurs showed a small reduction in trabecular bone volume in mice lacking PTH (irrespective of the CaSR status) which may confirm the histological data. However, it remains unclear what causes the increase in osteoclast numbers in animals lacking PTH:

In summary, *Casr*^BCH002 recapitulate major features of patients with FHH1. However, the analysis of double transgenic mice lacking also PTH, suggests that part of the syndrome are rather caused by direct effects of mutant *Casr* than by dysregulated PTH.

Declarations

Ethical approval All experiments were performed according to Swiss Animal Welfare laws and approved by the local veterinary authority (Kantonales Veterinäramt Zürich) under the numbers ZH156/16 and ZH240/19.

Competing interests CAW reports honoraria from Medice and Kyowa Kirin and collaborations with Chugai and Bayer AG outside this study.

References

1. Afzal M, Kathuria P (2023) Familial hypocalciuric hypercalcemia. In: StatPearls. StatPearls Publishing, Treasure Island (FL)
2. Ba J, Brown D, Friedman PA (2003) Calcium-sensing receptor regulation of PTH-inhibitable proximal tubule phosphate transport. Am J Physiol Renal Physiol 285:F1233-1243
3. Biber J, Stieger B, Stange G, Murer H (2007) Isolation of renal proximal tubular brush-border membranes. Nat Protoc 2:1356–1359. https://doi.org/10.1038/nprot.2007.156
4. Bouxsein ML, Boyd SK, Christiansen BA, Guldberg RE, Jepsen KJ, Muller R (2010) Guidelines for assessment of bone microstructure in rodents using micro-computed tomography. J Bone Miner Res 25:1468–1486. https://doi.org/10.1002/jbmr.141
5. Capasso G, Geibel PJ, Damiano S, Jaeger P, Richards WG, Geibel JP (2013) The calcium sensing receptor modulates fluid reabsorption and acid secretion in the proximal tubule. Kidney Int 84:277–284. https://doi.org/10.1038/ki.2013.137
6. Chavez-Canales M, Garcia JA, Gamba G (2023) Regulation of the WNK4-SPAK-NCC pathway by the calcium-sensing receptor. Curr Opin Nephrol Hypertens 32:451–457. https://doi.org/10.1097/MNH.0000000000000915
7. Collazo R, Fan L, Hu MC, Zhao H, Wiederkehr MR, Moe OW (2000) Acute regulation of Na+/H+ exchanger NHE3 by parathyroid hormone via NHE3 phosphorylation and dynamin-dependent endocytosis. J Biol Chem 275:31601–31608. https://doi.org/10.1074/jbc.M000600200
8. Custer M, Lotscher M, Biber J, Murer H, Kaissling B (1994) Expression of Na-P(i) cotransport in rat kidney: localization by RT-PCR and immunohistochemistry. Am J Physiol 266:F767-774. https://doi.org/10.1152/ajprenal.1994.266.5.F767
9. Daryadel A, Haykir B, Kung CJ, Bugarski M, Bettoni C, Schnitzbauer U, Hernando N, Hall AM, Wagner CA (2022) Acute adaptation of renal phosphate transporters in the murine kidney to oral phosphate intake requires multiple signals. Acta Physiol (Oxf) 235:e13815. https://doi.org/10.1111/apha.13815
10. Edwards A, Bonny O (2018) A model of calcium transport and regulation in the proximal tubule. Am J Physiol Renal Physiol 315:F942–F953. https://doi.org/10.1152/ajprenal.00129.2018
11. Fuente R, Gil-Pena H, Claramunt-Taberner D, Hernandez-Frias O, Fernandez-Iglesias A, Alonso-Duran L, Rodriguez-Rubio E, Hermida-Prado F, Anes-Gonzalez G, Rubio-Aliaga I, Wagner C, Santos F (2019) MAPK inhibition and growth hormone: a promising therapy in XLH. FASEB J 33:8349–8362. https://doi.org/10.1096/fj.201802007R
12. Girardi AC, Titan SM, Malnic G, Reboucas NA (2000) Chronic effect of parathyroid hormone on NHE3 expression in rat renal proximal tubules. Kidney Int 58:1623–1631
13. Graca JA, Schepelmann M, Brennan SC, Reens J, Chang W, Yan P, Toka H, Riccardi D, Price SA (2016) Comparative expression of the extracellular calcium-sensing receptor in the mouse, rat, and human kidney. Am J Physiol Renal Physiol 310:F518-533. https://doi.org/10.1152/ajprenal.00208.2015
14. Hannan FM, Kallay E, Chang W, Brandi ML, Thakker RV (2018) The calcium-sensing receptor in physiology and in calcitropic and noncalcitropic diseases. Nat Rev Endocrinol 15:33–51. https://doi.org/10.1038/s41574-018-0115-0
15. Ho C, Conner DA, Pollak MR, Ladd DJ, Kifor O, Warren HB, Brown EM, Seidman JG, Seidman CE (1995) A mouse model of human familial hypocalciuric hypercalcemia and neonatal severe hyperparathyroidism. Nat Genet 11:389–394. https://doi.org/10.1038/ng1295-389
16. Ling S, Shi P, Liu S, Meng X, Zhou Y, Sun W, Chang S, Zhang X, Zhang L, Shi C, Sun D, Liu L, Tian C (2021) Structural mechanism of cooperative activation of the human calcium-sensing receptor by Ca(2+) ions and L-tryptophan. Cell Res 31:383–394. https://doi.org/10.1038/s41422-021-00474-0
17. Loffing J, Vallon V, Loffing-Cueni D, Aregger F, Richter K, Pietri L, Bloch-Faure M, Hoenderop JG, Shull GE, Meneton P, Kaissling B (2004) Altered renal distal tubule structure and renal Na(+) and Ca(2+) handling in a mouse model for Gitelman's syndrome. J Am Soc Nephrol 15:2276–2288. https://doi.org/10.1097/01.ASN.0000138234.18569.63

18. Loupy A, Ramakrishnan SK, Wootla B, Chambrey R, de la Faille R, Bourgeois S, Bruneval P, Mandet C, Christensen EI, Faure H, Cheval L, Laghmani K, Collet C, Eladari D, Dodd RH, Ruat M, Houillier P (2012) PTH-independent regulation of blood calcium concentration by the calcium-sensing receptor. J Clin Invest 122:3355–3367. https://doi.org/10.1172/JCI57407

19. Miao D, He B, Karaplis AC, Goltzman D (2002) Parathyroid hormone is essential for normal fetal bone formation. J Clin Invest 109:1173–1182. https://doi.org/10.1172/JCI14817

20. Nowik M, Picard N, Stange G, Capuano P, Tenenhouse HS, Biber J, Murer H, Wagner CA (2008) Renal phosphaturia during metabolic acidosis revisited: molecular mechanisms for decreased renal phosphate reabsorption. Pflugers Arch 457:539–549. https://doi.org/10.1007/s00424-008-0530-5

21. Pollak MR, Brown EM, Chou YH, Hebert SC, Marx SJ, Steinmann B, Levi T, Seidman CE, Seidman JG (1993) Mutations in the human Ca(2+)-sensing receptor gene cause familial hypocalciuric hypercalcemia and neonatal severe hyperparathyroidism. Cell 75:1297–1303. https://doi.org/10.1016/0092-8674(93)90617-y

22. Prot-Bertoye C, Lievre L, Houillier P (2022) The importance of kidney calcium handling in the homeostasis of extracellular fluid calcium. Pflugers Arch 474:885–900. https://doi.org/10.1007/s00424-022-02725-4

23. Quinn SJ, Thomsen AR, Pang JL, Kantham L, Brauner-Osborne H, Pollak M, Goltzman D, Brown EM (2013) Interactions between calcium and phosphorus in the regulation of the production of fibroblast growth factor 23 in vivo. Am J Physiol Endocrinol Metab 304:E310-320. https://doi.org/10.1152/ajpendo.00460.2012

24. Renkema KY, Velic A, Dijkman HB, Verkaart S, van der Kemp AW, Nowik M, Timmermans K, Doucet A, Wagner CA, Bindels RJ, Hoenderop JG (2009) The calcium-sensing receptor promotes urinary acidification to prevent nephrolithiasis. J Am Soc Nephrol 20:1705–1713. https://doi.org/10.1681/ASN.2008111195

25. Riccardi D, Valenti G (2016) Localization and function of the renal calcium-sensing receptor. Nat Rev Nephrol 12:414–425. https://doi.org/10.1038/nrneph.2016.59

26. Sabrautzki S, Rubio-Aliaga I, Hans W, Fuchs H, Rathkolb B, Calzada-Wack J, Cohrs CM, Klaften M, Seedorf H, Eck S, Benet-Pages A, Favor J, Esposito I, Strom TM, Wolf E, Lorenz-Depiereux B, Hrabe de Angelis M (2012) New mouse models for metabolic bone diseases generated by genome-wide ENU mutagenesis. Mamm Genome 23:416–430. https://doi.org/10.1007/s00335-012-9397-z

27. Sands JM, Naruse M, Baum M, Jo I, Hebert SC, Brown EM, Harris HW (1997) Apical extracellular calcium/polyvalent cation-sensing receptor regulates vasopressin-elicited water permeability in rat kidney inner medullary collecting duct. J Clin Invest 99:1399–1405

28. Schnoz C, Carrel M, Loffing J (2020) Loss of sodium chloride co-transporter impairs the outgrowth of the renal distal convoluted tubule during renal development. Nephrol Dial Transplant 35:411–432. https://doi.org/10.1093/ndt/gfz172

29. van der Hagen EA, Lavrijsen M, van Zeeland F, Praetorius J, Bonny O, Bindels RJ, Hoenderop JG (2014) Coordinated regulation of TRPV5-mediated Ca(2)(+) transport in primary distal convolution cultures. Pflugers Arch 466:2077–2087. https://doi.org/10.1007/s00424-014-1470-x

30. Vimalraj S (2020) Alkaline phosphatase: Structure, expression and its function in bone mineralization. Gene 754:144855. https://doi.org/10.1016/j.gene.2020.144855

31. Wagner CA, Loffing-Cueni D, Yan Q, Schulz N, Fakitsas P, Carrel M, Wang T, Verrey F, Geibel JP, Giebisch G, Hebert SC, Loffing J (2008) Mouse model of type II Bartter's syndrome. II. Altered expression of renal sodium- and water-transporting proteins. Am J Physiol Renal Physiol 294:F1373-1380. https://doi.org/10.1152/ajprenal.00613.2007